Mathematical and Computational Applications

MDPI

Article

Prescribed Performance Adaptive Backstepping Control for Winding Segmented Permanent Magnet Linear Synchronous Motor

Weiming Zhang *, Dapan Li, Xuyang Lou and Dezhi Xu

School of Internet of Things Engineering, Jiangnan University, Wuxi 214122, China; 17826110821@163.com (D.L.); Louxy@jiangnan.edu.cn (X.L.); xudezhi@jiangnan.edu.cn (D.X.)

* Correspondence: wmzhang21@163.com

Received: 10 February 2020; Accepted: 26 March 2020; Published: 27 March 2020

Abstract: In this paper, a prescribed performance adaptive backstepping control (PPABC) strategy is proposed to control the speed of a winding segmented permanent magnet linear synchronous motor (WS-PMLSM) with variable parameters and an unknown load disturbance. Firstly, a mathematical model of WS-PMLSM is provided. Then, the prescribed performance technique is introduced in the adaptive backstepping control to improve the transient performance and ensures the tracking error converges within a predetermined range. In addition, a constrained command filter is introduced to address the problem of differential expansion which exists in the traditional backstepping method, and a filter compensation signal is designed against the filter error. Moreover, the adaptive law is designed based on Lyapunov stability theory to estimate the uncertainties caused by parameter changes and load disturbances. The stability of the proposed control strategy is given and the simulation of the control system is carried out under the proposed PPABC in contrast with another backstepping control and traditional PI control. Finally, the experiment is conducted to further show the effectiveness of the proposed controller.

Keywords: prescribed performance; constrained command filter; backstepping; WS-PMLSM

1. Introduction

In recent years, the linear motor (LM) is widely used in many fields such as machine tools [1], vehicles [2], and workshop transportations [3]. In terms of its structure, there are no intermediate devices like screws and gears inside the LM since its working process doesn't contain conversion from rotational motion to linear motion which is required in the conventional rotary motor. Hence, the mechanical loss exhibits little in the LM, which makes LM more popular in the field of linear motion [4,5]. In addition, LM also possesses many other advantages, such as high precision, high efficiency, low noise, simple mechanism, and high power density [2]. Compared with linear induction motors, permanent magnet synchronous linear motors (PMLSMs) are more efficient and have a higher power density [3]; thus, they are widely used in high quality linear motion systems. PMLSMs can be divided into two categories according to their structural characteristics: long primary short secondary and long secondary short primary. The latter requires that the driven cable moves with the secondary mover, which reduces the reliability of the system and limits the speed of the secondary mover. The long primary winding needs a high supply voltage due to its length which results in excessive resistance and inductance, producing a large electromagnetic loss [6]. To overcome the shortcomings of traditional long primary PMLSMs, a winding segmented permanent magnet linear synchronous motor (WS-PMLSM) is proposed. The WS-PMLSM basically decomposes a high-power linear motor into multiple low-power linear motor units, in order to avoid powering the whole primary winding. The drive system only needs to drive the primary sections coupled with the mover,

reducing the pressure on the drive system and improving the efficiency. Additionally, in terms of manufacturing and maintenance, the modular segmented structure of the primary winding has the advantages of flexible topology, convenient fabrication, ease of manufacture, assembly and disassembly, adjustable stroke length, and easy maintenance [6]. However, many parameters of WS-PMLSM are variable due to its special structure, such as the resistance which varies with temperature and the three-phase unbalance. In particular, when the mover is coupled with the two segments at the same time, the flux and inductance of the primary winding changes with the position of the mover. The uncertainty of the motor parameters makes control difficult, and it is obviously difficult to achieve a good control effect of the WS-PMLSM using traditional PI control.

In recent years, scholars have done a lot of research on WS-PMLSM. In [6], the effect on inductance and magnetic field was studied due to winding section and the position of the mover changes. In [7], the influence of inductance and flux linkage variation on control performance was researched. In [8], an adaptive backstepping method was proposed using an adaptive rate that was designed based on Lyapunov stability theory to handle the parameter variation, in order to eliminate the influence of parameter uncertainty of the control system. However, this method did not consider differential expansion; the designed controller was too large for calculation and difficult to use in practical applications. Additionally, it did not consider the dynamic performance of the system. In [9,10], the controller was designed based on predictive control and achieve good control performance; however, this control method was too large in calculation, which limited its application in practice. In [11], a new control method was proposed based on support vector machine and direct torque control, but this method has a large thrust ripple.

Backstepping has been widely used in motor control due to its easy combination with other control techniques such as adaptive control and slide structure control. Backstepping control can achieve complete decoupling of the PMLSM [12], and a controller based on backstepping has global stability [13]. However, traditional backstepping control requires accurate model information and cannot adapt to parameters that are changing with time [14–16]. In order to improve the robustness of traditional backstepping control, adaptive control [17–19] and sliding structure control [20–23] have been introduced to manage the uncertainties and nonlinearity, and these methods have achieved good control effect. In [10], a sliding structure method was proposed, which applied the sliding mode structure method to adaptive backstepping control. The proposed method could enhance the dynamic performance of the system, but the sliding mode variable structure control caused shake, especially at low speeds. However, neither of these control methods considered the input limitation problem. When there are limited inputs, the controller designed by either method may be unstable, limiting its use in practical applications.

In this paper, prescribed performance and constrained command filter are introduced to adaptive backstepping control. The command filter is introduced to address input limitation and differential expansion [24–26]. Prescribed performance is introduced to improve dynamic performance by taking transient performance such as overshoots and adjustment time into consideration to ensure that the tracking error converges to a prescribed area within a prescribed time [27–29]. The advantages of the controller designed in this paper are as follows: 1. A constrained command filter is implemented in the backstepping control to handle differential expansion. 2. The constrained command filter limits the amplitude and rate of change of the virtual control signal, ensuring that the signal satisfies the constraints of the system and enhancing its practicability. 3. The prescribed performance method considers transient performance of the error based on stability error analysis, thus enhancing the dynamic performance of the system.

2. Mathematical Model of Winding Segmented Permanent Magnet Linear Synchronous Motor

2.1. Mathematical Model of PMLSMs

The structure of WS-PMLSM is shown as Figure 1. Ignoring the influence of the PMLSM flux leakage and harmonics in the gap magnetic field, the gap magnetic field generated by the permanent magnet has a positive dark wave distribution, and the expression of air gap flux is:

$$B(x) = \begin{cases} B_m \sin((x-r)\pi/\tau) & 0 \le x < l \\ 0 & \text{others} \end{cases} \tag{1}$$

where B_m is the max gap flux, x is the position of mover, l is the length of mover, τ is pole pitch, and r is the half coupling length of the mover.

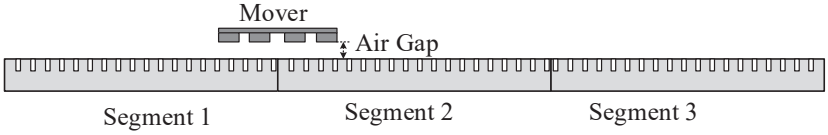

Figure 1. Structure of the WS-PMLSM.

When the mover is moving at speed v, the relationship between the induced electromotive force in the primary winding and the position of the mover is:

$$E = -vN_c \frac{d\psi}{dt} = -vN_c \frac{d}{dt} \int_{x1}^{x2} B(x) l dx \tag{2}$$

where E is the induced electromotive force and N_c is the number of coil turns.

Based on the position of the mover, the induced electromotive force can be written uniformly as:

$$E = \begin{cases} 0 & r > x_2 \text{ or } r < x_1 - l \\ -vN_c B_m \sin\left((x_2 - r)\,\pi/\tau\right) l & x_1 < r < x_2 \\ -vN_c B_m \sin\left((x_2 - r)\,\pi/\tau - (x_1 - r)\,\pi/\tau\right) l & x_2 - l < r < x_1 \\ -vN_c B_m \sin\left((x_1 - r)\,\pi/\tau\right) l & x_1 - l < r < x_2 - l \end{cases} \tag{3}$$

The primary winding's induced electromotive force is the sum of the induced electromotive forces of each coil and the induced electromotive force of the primary winding is given as:

$$\sum E = E_1(r) + E_2(r) + \ldots + E_n(r) \tag{4}$$

As the mover gradually enters or leaves a segment, the number of coupled coils changes with the position of the mover, causing instability due to an electromagnetic thrust in the single primary segment. By considering the process of the mover as it moves between the two primary windings, the electromagnetic thrust of the primary can be obtained as the result of the combined action of the two adjacent primary segments, as the mover is coupled with two adjacent segments at the same time. Thus, the electromagnetic thrust of the primary is:

$$\sum F = \frac{1}{2v}\left((E_{a1}I_{a1} + E_{b1}I_{b1} + E_{c1}I_{c1}) + (E_{a2}I_{a2} + E_{b2}I_{b2} + E_{c2}I_{c2})\right) \tag{5}$$

If the currents in both adjacent segments are maintained at exactly the same magnitude and phase, the electromagnetic thrust can be rewritten as:

$$\sum F = \frac{1}{2v}\left((E_{a1} + E_{a2})I_a + (E_{b1} + E_{b2})I_b + (E_{c1} + E_{c2})I_c\right) \tag{6}$$

It can be obtained from (3), (4), and (6) that, as long as the coupling area of the primary winding and the secondary actuator is constant, the electromagnetic thrust remains stable while the mover is moving in and out of the adjacent segment. The primary winding consists of multiple segments which are each powered and controlled independently. Unlike a traditional PMLSM, many parameters of WS-PMLM change depending on the relative position between the primary and mover while the mover is moving. This change causes variation in the electromagnetic parameters of the segment which are a function of the mover position. As the mover moves in or out or each segment, the mover magnetic field affects the segment magnetic field. As the coupling area increases, the magnetic reluctance, the self-inductance, the mutual inductance, and the excitation electromotive force of the segment shows an upward trend. When the mover moves completely over the segment and the magnetic circuit is fully coupled, the magnetic reluctance of the segment and the amplitude of the self-inductance, the mutual inductance and the excitation electromotive force remain stable and there is no further change. As the mover exits the segment and the coupling area decreases, the magnetic reluctance of the segment and the amplitude of the self-inductance, the mutual inductance and the excitation electromotive force show a downward trend. The mathematical model of the primary winding segmented permanent magnet linear motor is similar to the mathematical model of the conventional surface-mounted permanent magnet linear synchronous motor. The difference is that the parameter changes due to mover movement should be considered in WS-PMLSM. The motor parameters are related to the position of the mover. In order to simplify the expression of the mathematical model, the synchronous inductance and the permanent magnet flux are denoted by $L_s(x)$ and $\psi_f(x)$, respectively. The voltage equation of the WS-PMLSM segment in the d-q axis synchronous rotating coordinate system is:

$$\begin{cases} u_d = Ri_d + L(x)\frac{di_d}{dt} - vp\frac{\pi}{\tau}L(x)i_q \\ u_q = Ri_q + L(x)\frac{di_q}{dt} - vp\frac{\pi}{\tau}\left(L(x)i_d + \psi_f(x)\right) \end{cases} \tag{7}$$

where u_{d}, u_q, i_d, and i_q are the d-axis, q-axis voltage and d-axis, q-axis current, R is the primary winding resistance, and v is the mover movement speed. The electromagnetic thrust equation of the primary winding is described as:

$$F_e = \frac{3\pi}{2\tau}Pi_q\psi_f = K_T i_q \tag{8}$$

where F_e is the electromagnetic thrust, P is the number of pole pairs, and K_T is the thrust coefficient.

The dynamic equation of the secondary mover is described as:

$$F_e = T_l + M\frac{dv}{dt} + Bv \tag{9}$$

where T_l is the external disturbance term, M is the mass of the mover, and B is the friction coefficient.

As the WS-PMLSM motor parameters change with the position of the mover, its parameters cannot be accurately obtained, and the WS-PMLSM motor model equation can be rewritten as:

$$\begin{cases} \dot{i}_d = \frac{1}{L}u_d - \frac{R}{L}i_d + vp\frac{\pi}{\tau}i_q + \beta_1 \\ \dot{i}_q = \frac{1}{L}u_q - \frac{R}{L}i_q - v\frac{\pi}{\tau}i_d - \frac{vp\pi\psi_f}{L\tau} + \beta_2 \\ F_e = M\dot{v} + Bv + T_l + \beta_3 \end{cases} \tag{10}$$

where β_1, β_2, and β_3 are error variables.

3. Prescribed Performance Adaptive Backstepping Controller Designer

3.1. Constrained Command Filter

The backstepping control method should differentiate the level of virtual control required incrementally as differential expansion occurs. Since actuator saturation can occur in practical applications, this paper uses a constrained command filter, which addresses the differential expansion and controller saturation. The mathematical form of its state space model is described as [30]:

$$\begin{bmatrix} \dot{q}_1 \\ \dot{q}_2 \end{bmatrix} = \begin{bmatrix} q_2 \\ 2\xi\omega_n \left[S_R \left(\frac{\omega_n^2}{2\xi\omega_n} \left(S_M(u) - q_1 \right) \right) - q_2 \right] \end{bmatrix} \tag{11}$$

where $[q_1, q_2]^T = [x^c, \dot{x}^c]^T$ is magnitude limit. The structure of constrained command filter is defined as in Figure 2.

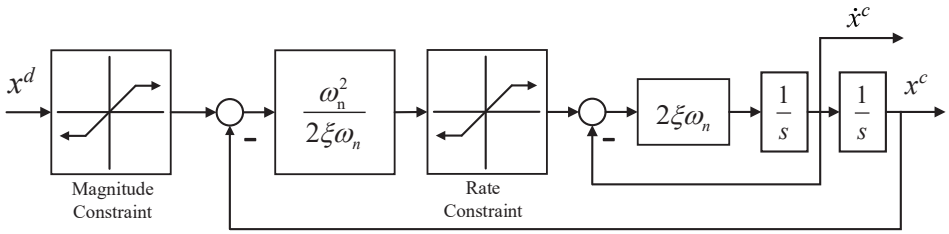

Figure 2. Constrained command filter structure.

The constrained command filter can solve the problems of differential expansion and controller saturation but will produce a filtering error [31] $\eta = i_q^c - i_q^d$, which will interfere with the performance of the controller and should be taken into consideration. In this paper, a filter compensator signal is introduced to eliminate this error which can be defined as:

$$\dot{\eta} = -k\eta + \frac{K_T}{M}(i_q^c - i_q^d) \tag{12}$$

where i_q^d is the given q-axis primary current, i_q^c is the output of the constrained command filter, and k is a positive scalar.

3.2. Prescribed Performance Function and Error Transformation

In order to obtain the prescribed control performance, a prescribed performance method is proposed which bounds the tracking error of the system by the prescribed performance. The definition of the prescribed performance function is given as follows [32,33]:

Definition 1. *A smooth function $\rho(t) : \mathcal{R}^+ \to \mathcal{R}^+$ that satisfies the following two conditions can be used as prescribed performance function:*

1. *$\rho(t)$ is positive and strictly decreasing.*
2. $\lim_{t\to\infty} \rho(t) = \rho_\infty > 0$

In this paper, a prescribed performance function is selected as:

$$\rho(t) = (\rho_0 - \rho_\infty)e^{-lt} + \rho_\infty \tag{13}$$

where ρ_0, ρ_∞, and l are positive constants.

The speed tracking error is defined as follows:

$$e_1(t) = v(t) - v^c(t) \tag{14}$$

where $v^c(t)$ is the given speed. In addition, $v^c(t)$ must be continuous and be derivable, and $\dot{v}^c(t)$ must be continuous and derivable and bounded. The defined compensated track error is:

$$\bar{e}_1(t) = e_1(t) - \eta \tag{15}$$

In order to ensure that the compensated error meets the prescribed static and dynamic performance, the compensated track error $\bar{e}_1(t)$ is bounded by the following criteria:

$$\begin{cases} -N\rho(t) < \bar{e}_1(t) < \rho(t), & \bar{e}_1(0) > 0 \\ -\rho(t) < \bar{e}_1(t) < N\rho(t), & \bar{e}_1(0) < 0 \end{cases} \tag{16}$$

where $0 \leq N \leq 1$.

According to (13) and (16), at time $t = 0$, if the compensated error $\bar{e}_1(t)$ satisfies function (16), the performance of the compensated track error $\bar{e}_1(t)$is governed by $\rho(t)$, and the convergence speed of $\bar{e}_1(t)$ is determined by $\rho(t)$ as well.

In order to convert the inequality to equation form, a conversion function is introduced to the prescribed performance function. The error transformation function is defined as:

$$\bar{e}_1(t) = \rho(t)\mathcal{L}(\varepsilon(t)) \tag{17}$$

where $\varepsilon(t)$ is the transformed error, and $\mathcal{L}(.)$ is a smooth and strictly increasing function which must meet the following two functions:

$$\begin{cases} -N < \mathcal{L}(\varepsilon) < 1, \bar{e}_1(0) > 0 \\ -1 < \mathcal{L}(\varepsilon) < N, \bar{e}_1(0) < 0 \end{cases} \tag{18}$$

$$\begin{cases} \lim\limits_{\varepsilon \to -\infty} \mathcal{L}(\varepsilon) = -M \\ \lim\limits_{\varepsilon \to \infty} \mathcal{L}(\varepsilon) = 1 \end{cases} \quad \bar{e}_1(0) > 0$$
$$\begin{cases} \lim\limits_{\varepsilon \to -\infty} \mathcal{L}(\varepsilon) = -1 \\ \lim\limits_{\varepsilon \to \infty} \mathcal{L}(\varepsilon) = M \end{cases} \quad \bar{e}_1(0) < 0 \tag{19}$$

In this paper, $\mathcal{L}(\varepsilon)$ is selected as:

$$\mathcal{L}(\varepsilon) = \begin{cases} \frac{e^{\varepsilon} - Ne^{-\varepsilon}}{e^{\varepsilon} + e^{-\varepsilon}}, & \bar{e}_1(0) > 0 \\ \frac{Ne^{\varepsilon} - e^{-\varepsilon}}{e^{\varepsilon} + e^{-\varepsilon}}, & \bar{e}_1(0) < 0 \end{cases} \tag{20}$$

According to (17) and (20), $\varepsilon(t)$ can be rewritten as:

$$\varepsilon(t) = \mathcal{L}^{-1}\left(\frac{\bar{e}_1(t)}{\rho(t)}\right) \tag{21}$$

The derivative of $\varepsilon(t)$ and the following function can be obtained as:

$$\dot{\varepsilon} = \frac{\partial \mathcal{L}^{-1}}{\partial(\bar{e}_1/\rho)} \frac{1}{\rho}\left(\dot{\bar{e}}_1 - \frac{\dot{\rho}\bar{e}_1}{\rho}\right) \tag{22}$$

According to (15) and (22), following function can be achieved as:

$$\dot{\varepsilon} = \frac{\partial \mathcal{L}^{-1}}{\partial(\bar{e}_1/\rho)} \frac{1}{\rho} \left(\dot{v} - \dot{v}^c - \dot{\eta} - \frac{\dot{\rho}\bar{e}_1}{\rho} \right) = r \left(\dot{v} - \dot{v}^c - \dot{\eta} - \alpha \right) \tag{23}$$

where $r = \frac{\partial \mathcal{L}^{-1}}{\partial(\bar{e}_1/\rho)} \frac{1}{\rho}, \alpha = \frac{\dot{\rho}\bar{e}_1}{\rho}$.

3.3. Prescribed Performance Adaptive Backstepping Controller Designer

The WS-PMLSM model has nonlinear characteristics and its model parameters are uncertain. Since traditional PI control cannot get adequate control effects, in order to obtain accurate speed control, this paper designs a prescribed performance adaptive backstepping controller as follows:

Step 1. Define the Lyapunov function as:

$$V_1 = \frac{1}{2r}\varepsilon^2 \tag{24}$$

Then, the derivation of V_1 is obtained as:

$$\dot{V}_1 = \varepsilon\left(\frac{K_T}{M}e_q - \frac{Bv}{M} - \frac{\beta_3}{M} - \dot{v}_c + k\eta + \frac{K_T}{M}i_q^d + \alpha\right) \tag{25}$$

Select i_q and i_d as the virtual control variables to stabilize the velocity. With respect to function (25), the following function is chosen to stabilize the velocity:

$$i_q^d = \frac{M}{K_T}\left(-k_1\varepsilon + \frac{Bv}{M} + \frac{\beta_3}{M} + \dot{v}^c - k\eta - \alpha\right) \tag{26}$$

where i_q^d and i_d^d are the command currents and k_1 is a positive scalar.

Since the parameters β_1, β_2 and β_3 cannot be accurately obtained, they can be replaced with adaptive estimated values $\hat{\beta}_1, \hat{\beta}_2$, and $\hat{\beta}_3$.

Rewrite (26) as

$$i_q^d = \frac{M}{K_T}\left(-k_1\varepsilon + \frac{Bv}{M} + \frac{\hat{\beta}_3}{M} + \dot{v}^c - k\eta - \alpha\right) \tag{27}$$

In this paper, we choose $i_d^d = 0$. Then, substituting (26) into (25), it can be obtained that

$$\dot{V}_1 = \varepsilon\left(\frac{K_T}{M}e_q + \frac{\tilde{\beta}_3}{M} - k_1\varepsilon\right) = -k_1\varepsilon^2 + \frac{K_T}{M}e_q\varepsilon + \frac{\tilde{\beta}_3}{M}\varepsilon \tag{28}$$

Step 2. Defined the current loop error as follows:

$$\begin{aligned} e_2(t) &= i_q(t) - i_q^c(t) \\ e_3(t) &= i_d(t) \end{aligned} \tag{29}$$

In order to obtain the adaptive law of $\beta_1, \beta_2, and \beta_3$ and the current loop control rate, the second step of the Lyapunov equation is selected as

$$V_2 = V_1 + \frac{1}{2}{e_q}^2 + \frac{1}{2}{e_d}^2 + \frac{1}{2\gamma_1}\tilde{\beta}_1^2 + \frac{1}{2\gamma_2}\tilde{\beta}_2^2 + \frac{1}{2\gamma_3}\tilde{\beta}_3^2 \tag{30}$$

where γ_1, γ_2, and γ_3 are positive scalars, $\tilde{\beta}_1$=$\beta_1 - \hat{\beta}_1$, $\tilde{\beta}_2$=$\beta_2 - \hat{\beta}_2$ and $\tilde{\beta}_3$=$\beta_3 - \hat{\beta}_3$ are the errors in the estimated parameters. The derivation of V_2 is taken as:

$$\dot{V}_2 = \varepsilon\left(\frac{K_T}{M}e_q - k_1\varepsilon + \frac{\tilde{\beta}_3}{M}\right) + e_q(\dot{i}_q - \dot{i}_q^c) + e_d\dot{i}_d + \frac{1}{\gamma_1}\tilde{\beta}_1\dot{\hat{\beta}}_1 + \frac{1}{\gamma_2}\tilde{\beta}_2\dot{\hat{\beta}}_2 + \frac{1}{\gamma_3}\tilde{\beta}_3\dot{\hat{\beta}}_3 \tag{31}$$

Substituting (10) into (31), we can obtain that:

$$\begin{aligned}\dot{V}_2 = &-k_1\varepsilon^2 + e_q\left(\tfrac{K_T}{M}\varepsilon + \tfrac{1}{L}u_q - \tfrac{R}{L}i_q - \tfrac{vp\pi\psi_f}{L\tau} + \hat{\beta}_2 - \dot{i}_q^c - v\tfrac{\pi}{\tau}i_d\right) + e_d\left(\tfrac{1}{L}u_d - \tfrac{R}{L}i_d + vp\tfrac{\pi}{\tau}i_q + \hat{\beta}_1\right)\\ &+\tfrac{1}{\gamma_1}\tilde{\beta}_1\left(\dot{\hat{\beta}}_1 - \gamma_1 e_d\right) + \tfrac{1}{\gamma_2}\tilde{\beta}_2\left(\dot{\hat{\beta}}_2 - \gamma_2 e_q\right) + \tfrac{1}{\gamma_3}\tilde{\beta}_3\left(\dot{\hat{\beta}}_3 + \gamma_3\tfrac{\varepsilon}{M}\right)\end{aligned} \tag{32}$$

According to (32), the current loop control law is designed as:

$$\begin{cases} u_q^d = -\frac{LK_T}{M}\varepsilon + Ri_q + \frac{vp\pi\psi_f}{\tau} - L\hat{\beta}_2 + Li_q^c + \frac{Lvp\pi}{\tau}i_d - k_2e_q \\ u_d^d = Ri_d - \frac{Lv\pi}{\tau}i_q - L\hat{\beta}_1 - k_3e_d \end{cases} \tag{33}$$

where u_q^d and u_d^d are the command voltage.

According to (32), the update laws for parameter error estimation can be obtained as:

$$\begin{cases} \dot{\hat{\beta}}_1 = \gamma_1 e_d \\ \dot{\hat{\beta}}_2 = \gamma_2 e_q \\ \dot{\hat{\beta}}_3 = -\gamma_3\frac{\varepsilon}{M} \end{cases} \tag{34}$$

Substituting (33) and (34) into (32), the following result can be obtained as:

$$\dot{V}_2 = -k_1\varepsilon^2 - k_2e_q^2 - k_3e_d^2 < 0 \tag{35}$$

3.4. Stability Analysis

Theorem 1. *The designed controllers and parameter adaptive laws designed according to (26), (33), and (34) ensure that all signals are bounded, thus ensuring that the compensation error meets the prescribed static and dynamic performance.*

Further analysis can provide the following conclusions:

Corollary 1.

$$\lim_{t\to\infty}|\bar{e}_1| = \lim_{t\to\infty}\left|i_q - i_q^c - \eta\right| = 0 \tag{36}$$

Proof. (1) If the command filter is not saturated, it can be obtained from (12) that $\lim_{t\to\infty}|\eta| = 0$. Therefore, it can be obtained by Theorem 1 that:

$$\lim_{t\to\infty}|\bar{e}_1| = \lim_{t\to\infty}\left|i_q - i_q^c - \eta\right| = 0$$

(2) If the command filter is saturated, based on LaSalle–Yoshizawa Theorem [34] and (35), the following conclusion can be obtained:

$$\lim_{t\to\infty}|\bar{e}_1| = \lim_{t\to\infty}\left|i_q - i_q^c - \eta\right| = 0$$

□

Based on Theorem 1 and Corollary 1, the following theorem can be obtained that:

Theorem 2. *(1)* $\lim_{t\to\infty} |\bar{e}_1| = 0$

(2) Tracking error e_1 *satisfies the following inequality:*

$$|e_1| \le |\mathcal{L}|\,|\rho| \sqrt{\sum_{i=1}^{3} \frac{1}{2\gamma_i} \tilde{\beta}_i(0)\hat{\beta}_i(0)} + \frac{|e_q|\,\frac{k_T}{M}}{2k} \tag{37}$$

Proof. (1) The first part has already been proven by Theorem 1.

(2) In light of (35) and Theorem 1, the following inequality can be obtained:

$$\varepsilon_1^2 \le \frac{1}{k_1}\left(V_2(0) - V_2(\infty)\right) \le \frac{1}{k_1} V_2(0) \tag{38}$$

Initial $\varepsilon(0) = e_q(0) = e_d(0) = 0$, and following equation can be obtained:

$$V_2(0) = V_1(0) + \frac{1}{2}e_q(0)^2 + \frac{1}{2}e_d(0)^2 + \frac{1}{2\gamma_1}\tilde{\beta}_1(0)^2 + \frac{1}{2\gamma_2}\tilde{\beta}_2(0)^2 + \frac{1}{2\gamma_3}\tilde{\beta}_3(0)^2 \tag{39}$$

Combining (38) with (39), it can be obtained as follows:

$$|\varepsilon| \le \sqrt{\sum_{i=1}^{3} \frac{1}{2\gamma_i} \tilde{\beta}_i(0)\hat{\beta}_i(0)} \tag{40}$$

As $\varepsilon(t) = \mathcal{L}^{-1}\left(\frac{\bar{e}_1(t)}{\rho(t)}\right)$ and $\mathcal{L}^{-1}$ is a monotonic and bounded function, it can be obtained as follows:

$$|\bar{e}_1| \le |\mathcal{L}| \sqrt{\sum_{i=1}^{3} \frac{1}{2\gamma_i} \tilde{\beta}_i(0)\hat{\beta}_i(0)}\,|\rho| \tag{41}$$

Then, the Lyapunov function is defined as

$$V_\eta = \frac{1}{2}\eta^2 \tag{42}$$

Take the derivation of V_2 as:

$$\dot{V}_\eta = \eta\dot{\eta} = -k\eta^2 + \eta\left(\frac{K_T}{M}(i_q^c - i_q^d)\right) \tag{43}$$

The following inequation can be obtained as:

$$\dot{V}_\eta \le -\left(k\eta - \frac{\frac{K_T}{M}(i_q^c - i_q^d)}{2k}\right)^2 + \left(\frac{\frac{K_T}{M}(i_q^c - i_q^d)}{2k}\right)^2 \tag{44}$$

Similarly, the following conclusions can be obtained as:

$$|\eta|^2 \le V_\eta(0) - V_\eta(\infty) + \left(\frac{\frac{K_T}{M}(i_q^c - i_q^d)}{2k}\right)^2 \tag{45}$$

Defining $\eta(0) = 0$, $V_\eta(0) = 0$, it can be obtained that:

$$|\eta| \le \left(\frac{\frac{K_T}{M}(i_q^c - i_q^d)}{2k}\right) \tag{46}$$

Thus, we can get the final result as

$$|e_1| \leq |\mathcal{L}| \sqrt{\sum_{i=1}^{3} \frac{1}{2\gamma_i} \tilde{\beta}_i(0)\hat{\beta}_i(0)}\, |\rho| + \frac{|e_q| \frac{k_T}{M}}{2k} \tag{47}$$

□

When the input is limited, the tracking error can be reduced by adjusting $\mathcal{L}$ and ρ in the method proposed in this paper. This is in contrast with the traditional backstepping method that can only reduce the tracking error by increasing the gains k_1 or adjusting the initial value of the adaptive function. PPABC has obvious advantages compared with the traditional backstepping method. The introduction of the prescribed performance method reduces the tracking error due to both signal limitations and filter errors and compensates for the deficiencies of traditional command filtering backstepping. Additionally, the traditional prescribed performance function limits the steady-state error within a certain range and requires that $\rho(\infty)$ is small enough in order to achieve high track precision.

4. Simulation Study

In this section, the effectiveness of the designed controller with respect to WS-PMLSM is verified via simulation. The parameters of the motor is listed in Table 1. In addition, according to the references and the parameters of the actual motor, disturbances such as inductance and flux changes are added to the simulation model to approximate the dynamic response of the actual motor. In order to clarify the control design process, a principle block diagram of the proposed control strategy is described in Figure 3.

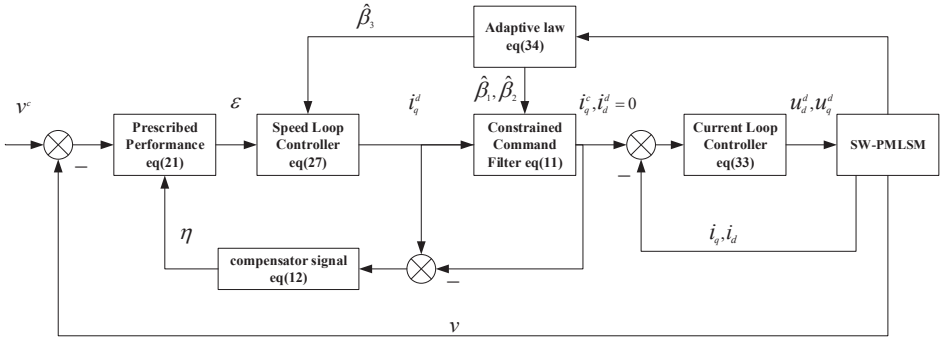

Figure 3. PPABC block diagram.

Table 1. Parameters of WS-PMLSM.

Definition	Parameter/Measure	Value
Mass	M/kg	3.5
Magnetic flux	ψ_f/Wb	0.2
Friction coefficient	$B/(\mathrm{N}/(\mathrm{m} \cdot \mathrm{s}^{-1}))$	0.027
Inductance	L/H	0.1021
Resistance	R/Ω	6.2689
Pole pitch	τ/m	0.027
Number of pole pairs	P	2

In order to achieve suitable control effects, the parameters of PPABC strategy require proper adjustment. The main work is to design the parameter of prescribed performance function. During the parameter adjustment process, ρ_0 must be set larger than the maximum tracking error once the motor starts to work. However, if it is selected too large, the overshoot may be large as well, which requires a balance between the tracking performance and overshoot. Moreover, ρ_∞ is the required precision

when the system tends to be stable and l determines the convergence rate of the system. The larger l is, the faster the error converges, yet the maximum response capacity of the system should also be considered. On the other hand, during the design process of adaptive parameters, once the estimation error is generated, the corresponding adaptive parameters ought to be adjusted according to the error to make minimum impact on the system. Motivated by the aforementioned adjustment, the controller parameters are designed as $k = 500$, $k_1 = k_2 = k_3 = 10,000$, adaptive parameters are designed as $\gamma_1 = 10000, \gamma_2 = 100,000, \gamma_3 = 10,000$, the prescribed performance function is designed as $\rho(t) = (1 - 0.005)e^{-90t} + 0.005$ and the constrained command filter is designed with $\omega = 3000, \xi = 0.1$, current magnitude limit is designed as ± 10 A and current rate limit is designed as ± 500 A/s.

Based on the above parameter adjustment, the simulation results are obtained. The compensated error $\bar{e}_1$ curves are shown in Figure 4. It is clear that the compensated error is bounded by the prescribed performance function and gradually converges to zero which indicates the stability of the system. In Figure 5, it is shown that the compensated error $\bar{e}_1$ still possesses quick response, fast convergence rate and stable state when the mass of mover turns to $3M$, which demonstrates that the controller designed in this paper owns robustness against parameter changes.

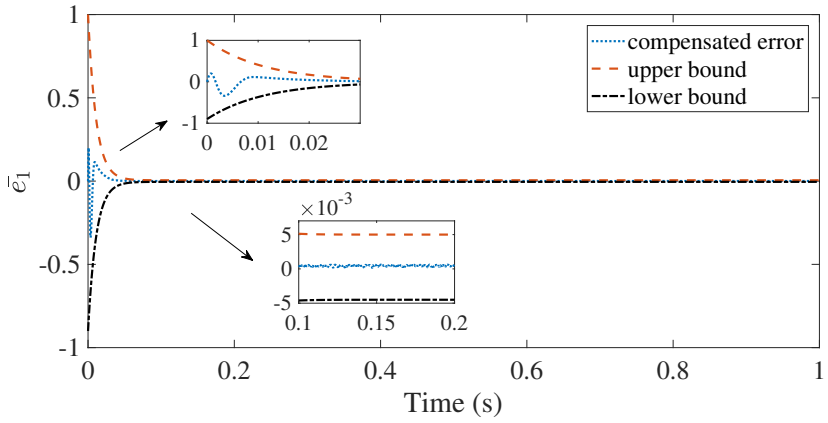

Figure 4. Compensated error curve.

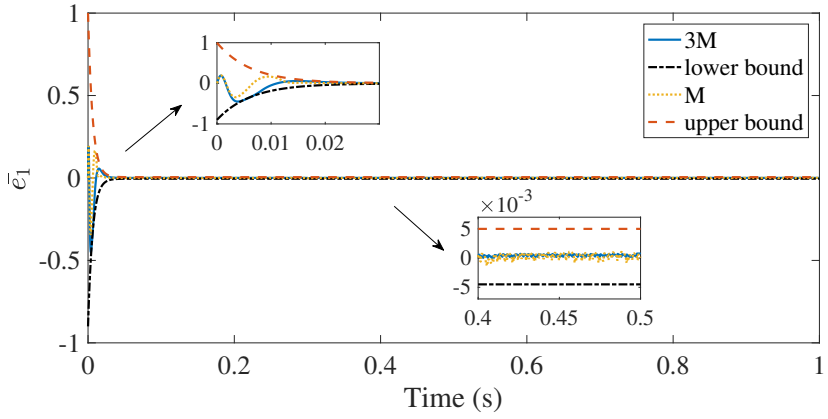

Figure 5. Compensated error curve with different mass.

The speed tracking performances of the proposed controller are shown in Figures 6 and 7, and the adaptive backstepping control (ABC) strategy in [8] and the conventional PI control are also applied to the system for comparison. It can be observed from Figure 6 that the speed under the proposed PPABC and ABC both have shorter convergence time and less overshoot than the conventional PI control, which verifies the effectiveness of the adaptive backstepping technique. However, the proposed PPABC exhibits less overshoot at the beginning and stays more stable than the ABC when the external

load disturbance occurs at 0.3 s owing to the introduction of the prescribed performance technique. In addition, Figure 7 presents the comparison more clearly from the point of view of error.

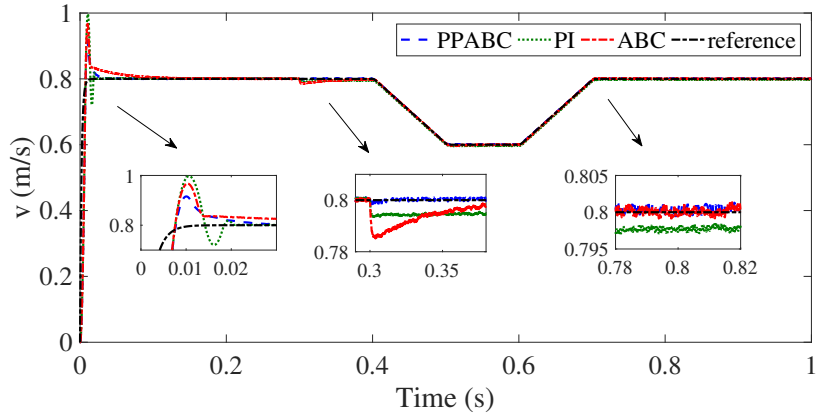

Figure 6. Speed tracking curves.

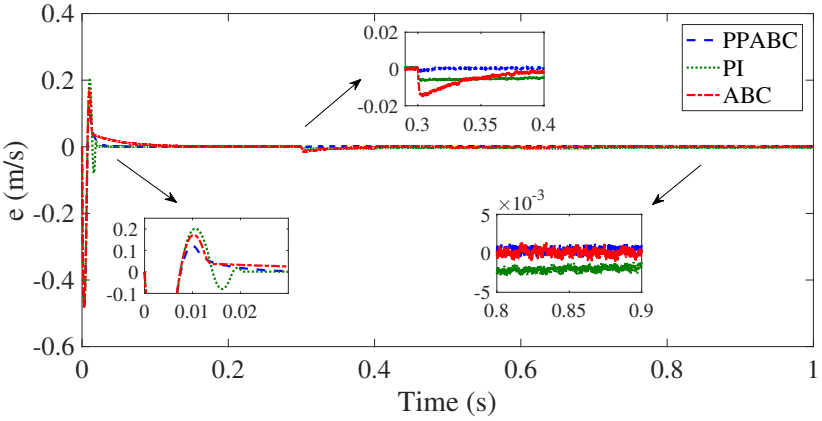

Figure 7. Speed error curves.

Similarly, the simulations with 3M mover mass are also carried out and the corresponding results are shown in Figures 8 and 9. It can be found that the speed under PPABC is kept stable regardless of the disturbance, which further demonstrates better robustness of the PPABC than ABC and PI. To sum up, the proposed PPABC owns better static and dynamic performance with quicker response, faster convergence rate, and better robustness than ABC and PI.

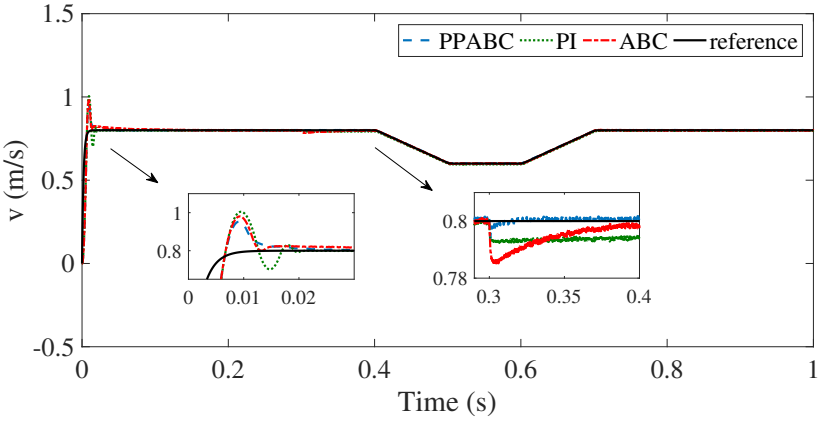

Figure 8. Speed tracking curves with 3M.

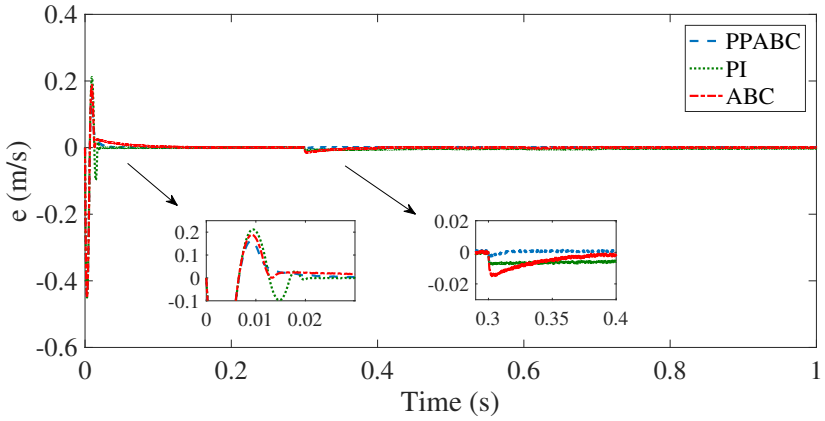

Figure 9. Speed error curves with 3*M*.

5. Experiment Validation

To further verify the effectiveness of the proposed algorithm, a physical experiment has been built, which is shown in Figure 10. The current signals are measured by hall sensors and the speed and position are measured by an incremental encoder, and the sampling period of velocity and current is 400 μs and 200 μs, respectively. The dead band is set to 5 μs.

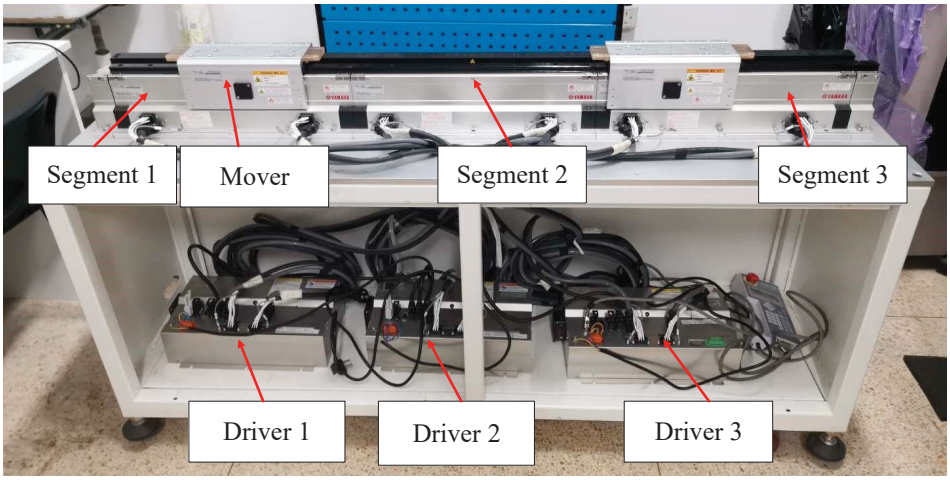

Figure 10. Configuration of experiment.

The reference speed is set to 1 m/s in the experiment. The speed control loop parameters of PI are $k_{vp} = 100, k_{vi} = 50$ and the q-axis current loop parameters are $k_{vp} = 200, k_{vi} = 80$, the d-axis current loop parameters are $k_{vp} = 150, k_{vi} = 60$. The main idea of parameter adjustment with respect to the proposed controller in the experiment is similar to that in simulation. In particular, the actual system suffers more disturbance, which makes the control accuracy lower than that in the simulation. Therefore, ρ_∞ in the experiment ought to be set larger than that designed in the simulation. In addition, there are differences in their inverter bridge, controller, and mathematical model which makes other parameters different between the simulation and the experiment. According to the above regulation, the parameters of PPABC controller in the experiment are designed as $k = 180$, $k_1 = k_2 = k_3 = 240$, the prescribed performance function is designed as $\rho(t) = (1 - 0.03)e^{-120t} + 0.03$.

The speed tracking performances are shown in Figures 11 and 12. As can be seen from experimental results, the response of the two control methods are roughly the same. However, the speed under the proposed PPABC owns a smaller overshoot than that under PI. In addition, it can be found that the steady fluctuation of the speed under the proposed method is smaller than PI, which validates the better static and dynamic performance of the proposed control strategy.

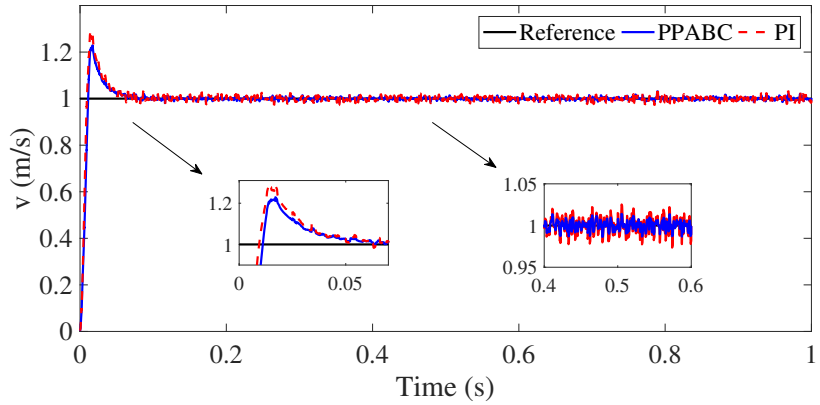

Figure 11. Speed tracking curve.

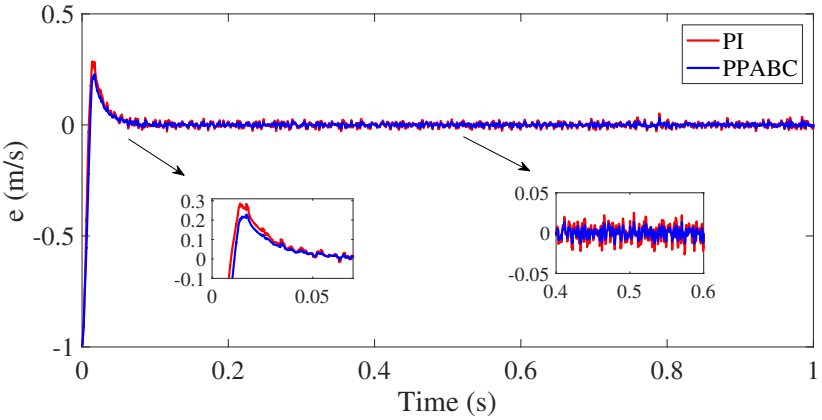

Figure 12. Speed tracking error curve.

6. Conclusions

In this paper, a PPABC strategy has been designed for WS-PWLSM, and the simulation and experiment results have proven that the controller can achieve precise velocity control of WS-PWLSM with parameter variation and external disturbances.

Firstly, a mathematical model of WS-PWLSM has been provided with the control strategy that drives two sections with the same current. Secondly, prescribed performance has been introduced to traditional backstepping control to ensure that the compensated error can converge within a predetermined range. The command filter has been also introduced to backstepping control to address the problem of differential expansion in the traditional backstepping algorithm. To address filter error, a compensation algorithm has also been introduced. Then, the PPABC has been designed according to Lyapunov stability theory and an adaptive law has been introduced to handle uncertain parameters and external disturbances. Finally, the simulation and experiment results prove that the proposed PPABC owns better static and dynamic performance with quicker response, faster convergence rate, and better robustness than ABC and PI.

Author Contributions: Conceptualization, W.Z. and D.L.; methodology, W.Z., D.L., and D.X.; software, W.Z. and X.L.; validation, D.L. and X.L.; investigation, W.Z., D.L., and D.X.; writing—original draft preparation, W.Z. and D.L.; writing—review and editing, W.Z., D.L, X.L., and D.X.; funding acquisition, W.Z. and D.X. All authors have read and agreed to the published version of the manuscript.

Funding: This work was partially supported by the Postgraduate Research & Practice Innovation Program of Jiangsu Province (SJCX19_0795), the National Natural Science Foundation of China (61973140, 61903158), the National First-Class Discipline Program of Food Science and Technology (JUFSTR20180205), and the National Science Foundation of Jiangsu Province of China (BK20180595).

Conflicts of Interest: The authors declare no conflict of interest.

References

1. Li, X.; Du, R.; Denkena, B.; Imiela, J. Tool breakage monitoring using motor current signals for machine tools with linear motors. *IEEE Trans. Ind. Electron.* **2005**, *52*, 1403–1408.
2. Lin, F.J.; Shen, P.H.; Hsu, S.P. Adaptive backstepping sliding mode control for linear induction motor drive. *IEE Proc. Electr. Power Appl.* **2002**, *149*, 184–194.
3. Yoshida, K.; Nakata, S.; Koga, S. Orthogonally switching motion control of PMLSM vehicle in mass-reduced mode. In Proceedings of the Sixth International Conference on Electrical Machines and Systems, Beijing, China, 9–11 November 2003; pp. 469–472.
4. Li, J.Q.; Li, W.L.; Deng, G.Q.; Ming, Z. Continuous-behavior and discrete-time combined control for linear induction motor-based urban rail transit. *IEEE Trans. Magn.* **2016**, *52*, 1–4.
5. Yue, F.; Li, X.; Chen, C.; Tan, W. Adaptive integral backstepping sliding mode control for opto-electronic tracking system based on modified LuGre friction model. *Int. J. Syst. Sci.* **2017**, *48*, 3374–3381.
6. Li, L.; Hong, J.; Lu, Z.; Ying, L.; Song, Y.; Liu, R.; Li, X. Fields and inductances of the sectioned permanent-magnet synchronous linear machine used in the EMALS. *IEEE Trans. Plasma Sci.* **2010**, *39*, 87–93, .
7. Ma, M.N.; Li, L.Y.; Zhu, H.; Chan, C.C. Inductance and Flux Linkage Variation on Operation Performance for Multi-Segmented Linear PM Motor. *Appl. Mech. Mater.* **2013**, *416*, 15–20.
8. Li, L.; Hong, J.; Wu, H.; Zhao, Z.; Li, X. Adaptive back-stepping control for the sectioned permanent magnetic linear synchronous motor in vehicle transportation system. In Proceedings of the 2008 IEEE Vehicle Power and Propulsion Conference, Harbin, China, 3–5 September 2008.
9. Hong, J.; Li, L.; Pan, D.; Zong, Z. Comparison of two current predictive control methods for a segment winding permanent magnet linear synchronous motor. In Proceedings of the 2012 16th International Symposium on Electromagnetic Launch Technology, Beijing, China, 15–19 May 2012.
10. Hong, J.; Li, L.; Zong, Z.; Liu, Z. Current error vector based prediction control of the section winding permanent magnet linear synchronous motor. *Energy Convers. Manag.* **2011**, *52*, 3347–3355.
11. Chen, L.; Zhu, H.; Sun, S.G.; Li, Y.Y.; Zhu, L.G. Inter-Stator Synchronous Combined Method Based on SVM-DTC for Primary Winding Discontinuous PMLSM. *Appl. Mech. Mater.* **2014**, *496*, 1394–1400.
12. Zhao, W.; Jiao, S.; Chen, Q.; Xu, D.; Ji, J. Sensorless control of a linear permanent-magnet motor based on an improved disturbance observer. *IEEE Trans. Ind. Electron.* **2018**, *65*, 9291–9300.
13. Peng, C.C.; Li, Y.; Chen, C.L. A robust integral type backstepping controller design for control of uncertain nonlinear systems subject to disturbance. *Int. J. Innov. Comput. Inf. Control* **2011**, *7*, 2543–2560.
14. Lin, F.J.; Hwang, J.C.; Chou, P.H. FPGA-based intelligent-complementary sliding-mode control for PMLSM servo-drive system. *IEEE Trans. Power Electron.* **2010**, *25*, 2573–2587.
15. Liu, H.; Pan, Y.; Li, S.; Chen, Y. Adaptive fuzzy backstepping control of fractional-order nonlinear systems. *IEEE Trans. Syst. Man Cybern. Syst.* **2017**, *47*, 2209–2217.
16. Hu, Q.; Shao, X.; Guo, L. Adaptive fault-tolerant attitude tracking control of spacecraft with prescribed performance. *IEEE ASME Trans. Mechatron.* **2017**, *23*, 331–341.
17. Yu, J.; Shi, P.; Dong, W.; Yu, H. Observer and command-filter-based adaptive fuzzy output feedback control of uncertain nonlinear systems. *IEEE Trans. Ind. Electron.* **2015**, *62*, 5962–5970.
18. Huang, P.; Wang, D.; Meng, Z.; Zhang, F.; Guo, J. Adaptive postcapture backstepping control for tumbling tethered space robot–target combination. *J. Guid. Control Dyn.* **2016**, *39*, 150–156.
19. Chen, C.P.; Wen, G.X.; Liu, Y.J.; Liu, Z. Observer-based adaptive backstepping consensus tracking control for high-order nonlinear semi-strict-feedback multiagent systems. *IEEE Trans. Cybern.* **2015**, *46*, 1591–1601.
20. Dhar, S.; Dash, P.K. Adaptive backstepping sliding mode control of a grid interactive PV-VSC system with LCL filter. *Sustain. Energy Grids Netw.* **2016**, *6*, 109–124.
21. Chen, F.; Jiang, R.; Zhang, K.; Jiang, B.; Tao, G. Robust backstepping sliding-mode control and observer-based fault estimation for a quadrotor UAV. *IEEE Trans. Ind. Electron.* **2016**, *63*, 5044–5056.
22. Xu, D.; Dai, Y.; Yang, C.; Yan, X. Adaptive fuzzy sliding mode command-filtered backstepping control for islanded PV microgrid with energy storage system. *J. Frankl. Inst.* **2019**, *356*, 1880–1898.

23. Zhang, L.; Tong, S.; Li, Y. Dynamic surface error constrained adaptive fuzzy output-feedback control of uncertain nonlinear systems with unmodeled dynamics. *Neurocomputing* **2014**, *143*, 123–133.
24. Shen, Q.; Shi, P. Distributed command filtered backstepping consensus tracking control of nonlinear multiple-agent systems in strict-feedback form. *Automatica* **2015**, *53*, 120–124.
25. Sonneveldt, L.; Chu, Q.P.; Mulder, J.A. Nonlinear flight control design using constrained adaptive backstepping. *J. Guid. Control Dyn.* **2007**, *30*, 322–336.
26. Dong, W.; Farrell, J.A.; Polycarpou, M.M.; Djapic, V.; Sharma, M. Command filtered adaptive backstepping. *IEEE Trans. Control Syst. Technol.* **2011**, *20*, 566–580.
27. Li, Y.; Tong, S.; Liu, L.; Feng, G. Adaptive output-feedback control design with prescribed performance for switched nonlinear systems. *Automatica* **2017**, *80*, 225–231.
28. Li, Y.; Tong, S. Adaptive neural networks prescribed performance control design for switched interconnected uncertain nonlinear systems. *IEEE Trans. Neural Netw. Learn. Syst.* **2017**, *29*, 3059–3068.
29. Huang, Y.; Na, J.; Wu, X.; Liu, X.; Guo, Y. Adaptive control of nonlinear uncertain active suspension systems with prescribed performance. *ISA Trans.* **2015**, *54*, 145–155.
30. Yu, J.; Shi, P.; Zhao, L. Finite-time command filtered backstepping control for a class of nonlinear systems. *Automatica* **2018**, *92*, 173–180.
31. Hu, J.; Zhang, H. Immersion and invariance based command-filtered adaptive backstepping control of VTOL vehicles. *Automatica* **2013**, *49*, 2160–2167.
32. Wang, M.; Yang, A. Dynamic learning from adaptive neural control of robot manipulators with prescribed performance. *IEEE Trans. Syst. Man Cybern. Syst.* **2017**, *47*, 2244–2255.
33. Bechlioulis, C.P.; Rovithakis, G.A. Prescribed performance adaptive control for multi-input multi-output affine in the control nonlinear systems. *IEEE Trans. Autom. Control* **2010**, *55*, 1220–1226.
34. Rouche, N.; Habets, P.; Laloy, M. *Stability Theory by Liapunov's Direct Method*; Springer-Verlag: New York, NY, USA, 1977.